Adam WOSATKO*

GRADIENT DAMAGE WITH VOLUMETRIC-DEVIATORIC DECOMPOSITION AND ONE STRAIN MEASURE

SUMMARY

The paper presents a two-field formulation of the gradient-enhanced damage model and its application. This isotropic model is characterized by two damage parameters with a volumetric-deviatoric decomposition. However, one strain measure governs the development of damage as for the scalar description. The theory is verified by means of one-element benchmarks and also a more sophisticated simulation, namely the splitting of concrete cylinder in the Brazilian test is discussed.

***Keywords**: isotropic damage, gradient enhancement, finite element method*

GRADIENTOWY MODEL MECHANIKI USZKODZEŃ Z AKSJATOROWO-DEWIATOROWĄ DEKOMPOZYCJĄ I JEDNĄ MIARĄ ODKSZTAŁCENIA

Artykuł przedstawia dwupolowe sformułowanie gradientowego modelu mechaniki uszkodzeń i jego zastosowanie. Ten izotropowy model charakteryzują dwa parametry uszkodzenia z podziałem aksjatorowo-dewiatorowym. Jednakże jedna miara odkształcenia decyduje o rozwoju uszkodzenia jak w opisie skalarnym. Teoria jest zweryfikowana za pomocą testów jednoelementowych, a także bardziej zaawansowanej symulacji rozłupywania betonowego cylindra w tzw. teście brazylijskim.

***Słowa kluczowe**: izotropowy model mechaniki uszkodzeń, model gradientowy, metoda elementów skończonych*

1. INTRODUCTION

In the simplest form of the damage theory one scalar parameter determines the degradation process. This definition of damage was firstly introduced in (Kachanov, 1958). Although this damage concept was proposed for isotropic continuum, it can be generalized introducing anisotropy. If damage directions are distinguished then one scalar parameter is insufficient. In the literature damage vectors (Krajcinovic and Fonseka 1981), second-order damage tensors (Murakami and Ohno 1981, Betten 1983, Litewka 1985) and fourth-order damage tensors (Chaboche 1981, Krajcinovic 1989, Lemaitre and Chaboche 1990) have been defined. Different descriptions of the damage theory can be found in (Skrzypek and Ganczarski 1999, Wu and Li 2008). However, numerical implementation of the theory with fourth-order damage tensors is complicated and a proper setup of material variables is difficult. On the other hand, the scalar model can be extended to two damage parameters (Ju 1990) remaining within the isotropic description. Some authors (Mazars and Pijaudier-Cabot 1989, Comi 2001) employ the modification where damage is decomposed into two parts related to tensile and compressive actions. However, the proposal discussed in this paper results from a volumetric-deviatoric split given for example in (Lubliner *et al.* 1989, Comi and Perego 2001). The first damage parameter influences the bulk modulus and the second one reduces the shear modulus. Hence two different damage growth functions are distinguished, but one damage history parameter and one damage loading function are assumed.

As a consequence, when the model it is applied in a gradient-enhanced format, one averaging equation is still the basis of a formulation of finite element method as for the scalar gradient damage (Peerlings *et al*. 1996). The theory is briefly discussed in Sections 2 and 3. The implemented model is first examined for one finite element, in Section 4. The next computational verification is performed in Section 5 by the simulation of the Brazilian cylinder split test. Final remarks are given in Section 6.

2. VOLUMETRIC-DEVIATORIC SPLIT

The continuum damage formulation satisfies the isotropy condition if two damage parameters ω_K and ω_G for the volumetric and deviatoric parts respectively are considered, cf. (Lubliner *et al.* 1989, Ju 1990, Comi and Perego 2001, Carol *et al.* 2002). The constitutive equation becomes:

$$\boldsymbol{\sigma} = \boldsymbol{E}_{\mathrm{KG}}\boldsymbol{\varepsilon} \tag{1}$$

where:

$$\boldsymbol{E}_{\mathrm{KG}} = (1-\omega_K)\, K\boldsymbol{\Pi}\boldsymbol{\Pi}^{\mathrm{T}} + 2(1-\omega_G)\, G\boldsymbol{Q} \tag{2}$$

Here $\boldsymbol{\sigma}$ is the stress tensor and $\boldsymbol{\varepsilon}$ is the strain tensor. Both are considered in a vector form and $\boldsymbol{\varepsilon} = [\varepsilon_{11}\ \varepsilon_{22}\ \varepsilon_{33}\ \varepsilon_{12}\ \varepsilon_{23}\ \varepsilon_{13}]^{\mathrm{T}}$. The damage parameter ω_K reduces bulk modulus K and the parameter ω_G degrades shear modulus G. The following relations are introduced:

$$\boldsymbol{Q} = \boldsymbol{Q}_0 - \frac{1}{3}\boldsymbol{\Pi}\boldsymbol{\Pi}^{\mathrm{T}} \tag{3}$$

$$\boldsymbol{Q}_{\mathrm{dev}} = \boldsymbol{I} - \frac{1}{3}\boldsymbol{\Pi}\boldsymbol{\Pi}^{\mathrm{T}} \tag{4}$$

where in three dimensions (3D): $\boldsymbol{\Pi} = [1, 1, 1, 0, 0, 0]^{\mathrm{T}}$ and $\boldsymbol{Q}_0 = diag\left[1, 1, 1, \frac{1}{2}, \frac{1}{2}, \frac{1}{2}\right]$.

* Cracow University of Technology, Faculty of Civil Engineering, Warszawska 24, Cracow, Poland; e-mail: awosatko@ L5.pk.edu.pl

Note that the strain and stress vectors are split into volumetric and deviatoric parts:

$$\varepsilon = \frac{1}{3}\boldsymbol{\Pi}\theta + \varepsilon_{\mathrm{dev}} \tag{5}$$

$$\boldsymbol{\sigma} = \boldsymbol{\Pi} p + \boldsymbol{\xi} \tag{6}$$

and the variables on the right-hand side are as follows: $\theta = \boldsymbol{\Pi}^{\mathrm{T}}\varepsilon$ is the dilatation, $\varepsilon_{\mathrm{dev}} = \boldsymbol{Q}\varepsilon$ is the deviatoric strain, $p = \frac{1}{3}\boldsymbol{\Pi}^{\mathrm{T}}\boldsymbol{\sigma}$ is the pressure and $\boldsymbol{\xi} = \boldsymbol{Q}_{\mathrm{dev}}\boldsymbol{\sigma}$ is the deviatoric stress. The stress rate is obtained differentiating (1):

$$\dot{\boldsymbol{\sigma}} = \boldsymbol{E}_{\mathrm{KG}}\dot{\boldsymbol{\varepsilon}} - \dot{\omega}_{\mathrm{K}} K \boldsymbol{\Pi}\boldsymbol{\Pi}^{\mathrm{T}}\boldsymbol{\varepsilon} - 2\dot{\omega}_{\mathrm{G}} G \boldsymbol{Q}\boldsymbol{\varepsilon} \tag{7}$$

One damage history parameter κ^{d} is adopted, i.e. $\kappa^{\mathrm{d}} = \kappa^{\mathrm{d}}_{\mathrm{K}} = \kappa^{\mathrm{d}}_{\mathrm{G}}$, so that one damage loading function:

$$f^{\mathrm{d}}(\boldsymbol{\varepsilon}, \kappa^{\mathrm{d}}) = \tilde{\varepsilon}(\boldsymbol{\varepsilon}) - \kappa^{\mathrm{d}} = 0 \tag{8}$$

is assumed. The Kuhn-Tucker conditions are satisfied by the equivalent strain measure $\tilde{\varepsilon}$ and the damage history parameter κ^{d}. This means that function $\tilde{\varepsilon}(\boldsymbol{\varepsilon})$ can be defined analogically to the scalar damage model.

However, two different damage growth functions are distinguished:

$$\omega_{\mathrm{K}} = \omega_{\mathrm{K}}(\kappa^{\mathrm{d}}) \tag{9}$$

$$\omega_{\mathrm{G}} = \omega_{\mathrm{G}}(\kappa^{\mathrm{d}}) \tag{10}$$

Since one history parameter κ^{d} governs the damage evolution, the rates of damage parameters ω_{K} and ω_{G} during loading are respectively:

$$\dot{\omega}_{\mathrm{K}} = \frac{\mathrm{d}\omega_{\mathrm{K}}}{\mathrm{d}\kappa^{\mathrm{d}}}\frac{\mathrm{d}\kappa^{\mathrm{d}}}{\mathrm{d}\tilde{\varepsilon}}\frac{\mathrm{d}\tilde{\varepsilon}}{\mathrm{d}\boldsymbol{\varepsilon}}\dot{\boldsymbol{\varepsilon}} \tag{11}$$

$$\dot{\omega}_{\mathrm{G}} = \frac{\mathrm{d}\omega_{\mathrm{G}}}{\mathrm{d}\kappa^{\mathrm{d}}}\frac{\mathrm{d}\kappa^{\mathrm{d}}}{\mathrm{d}\tilde{\varepsilon}}\frac{\mathrm{d}\tilde{\varepsilon}}{\mathrm{d}\boldsymbol{\varepsilon}}\dot{\boldsymbol{\varepsilon}} \tag{12}$$

and during unloading both $\dot{\omega}_{\mathrm{K}}$ and $\dot{\omega}_{\mathrm{G}}$ are equal to 0.

3. ISOTROPIC GRADIENT DAMAGE

It is by now common knowledge that the gradient enhanced model according to (Peerlings *et al.* 1996, Geers 1997, Pamin, 2004) is nonlocal. During a failure process, from the onset of localization until the total loss of the stiffness, the governing system of equations remains elliptic and the regularization allows one to avoid a spurious mesh sensitivity. This section concerns the derivation of isotropic damage with a gradient enhancement. The equations of the boundary value problem (BVP) are almost the same as for scalar damage, but the tangent stress-strain relation is defined in (7). Hence the averaging equation:

$$\bar{\varepsilon} - c\nabla^2\bar{\varepsilon} = \tilde{\varepsilon} \tag{13}$$

is still the basis of the two-field formulation like for the scalar gradient damage (Peerlings *et al.* 1996).

The above relation involves the second gradients of the averaged strain $\bar{\varepsilon}$. The parameter $c > 0$ has a unit of length squared and it is connected with the internal length scale l of a material. The relation $c = \frac{1}{2}l^2$ is derived for instance in (Askes *et al.* 2000). Instead of the local equivalent strain $\tilde{\varepsilon}$ the averaged strain $\bar{\varepsilon}$ now governs the damage progress:

$$f^{\mathrm{d}}(\boldsymbol{\varepsilon}, \kappa^{\mathrm{d}}) = \bar{\varepsilon}(\tilde{\varepsilon}(\boldsymbol{\varepsilon})) - \kappa^{\mathrm{d}} = 0 \tag{14}$$

The damage rates are computed as:

$$\dot{\omega}_{\mathrm{K}} = \frac{\partial\omega_{\mathrm{K}}}{\partial\kappa^{\mathrm{d}}}\frac{\partial\kappa^{\mathrm{d}}}{\partial\bar{\varepsilon}}\dot{\bar{\varepsilon}} = \mathcal{G}_{\mathrm{K}}\dot{\bar{\varepsilon}} \tag{15}$$

$$\dot{\omega}_{\mathrm{K}} = \frac{\partial\omega_{\mathrm{G}}}{\partial\kappa^{\mathrm{d}}}\frac{\partial\kappa^{\mathrm{d}}}{\partial\bar{\varepsilon}}\dot{\bar{\varepsilon}} = \mathcal{G}_{\mathrm{G}}\dot{\bar{\varepsilon}} \tag{16}$$

The weak form of equilibrium equations can be written as:

$$\int_{\mathcal{B}} \delta\boldsymbol{\varepsilon}^{\mathrm{T}}\boldsymbol{\sigma}\,\mathrm{d}V = \int_{\mathcal{B}} \delta\boldsymbol{u}^{\mathrm{T}}\boldsymbol{b}\,\mathrm{d}V + \int_{\partial\mathcal{B}} \delta\boldsymbol{u}^{\mathrm{T}}\boldsymbol{t}\,\mathrm{d}S \tag{17}$$

where $\boldsymbol{u}$ is the displacement field, $\boldsymbol{b}$ is the body force vector, $\boldsymbol{t}$ is the traction vector. A weak form of Equation (13) is derived using Green's formula and the homogeneous natural boundary condition: $(\nabla\bar{\varepsilon})^{\mathrm{T}}\boldsymbol{\nu} = 0$:

$$\int_{\mathcal{B}} \delta\bar{\varepsilon}\,\bar{\varepsilon}\,\mathrm{d}V + \int_{\mathcal{B}} (\nabla\delta\bar{\varepsilon})^{\mathrm{T}} c\nabla\bar{\varepsilon}\,\mathrm{d}V = \int_{\mathcal{B}} \delta\bar{\varepsilon}\,\tilde{\varepsilon}\,\mathrm{d}V \tag{18}$$

The two-field formulation involves independent interpolations of displacements u and averaged strain measure $\bar{\varepsilon}$ in the semi-discrete linear system. The primary fields are interpolated in this way:

$$\boldsymbol{u} = \boldsymbol{N}\boldsymbol{a} \quad \text{and} \quad \bar{\varepsilon} = \boldsymbol{h}^{\mathrm{T}}\boldsymbol{e} \tag{19}$$

where $\boldsymbol{N}$ and $\boldsymbol{h}$ contain suitable shape functions.

From the above interpolations the secondary fields can be computed in the following way:

$$\boldsymbol{\varepsilon} = \boldsymbol{B}\boldsymbol{a} \quad \text{and} \quad \nabla\bar{\varepsilon} = \boldsymbol{g}^{\mathrm{T}}\boldsymbol{e} \tag{20}$$

where $\boldsymbol{B} = \boldsymbol{L}\boldsymbol{N}$ ($\boldsymbol{L}$ is the standard differential operator matrix) and $\boldsymbol{g}^{\mathrm{T}} = \nabla\boldsymbol{h}^{\mathrm{T}}$. The discretized equations must hold for any admissible $\delta\boldsymbol{a}$ and $\delta\boldsymbol{e}$, therefore:

$$\int_{\mathcal{B}} \boldsymbol{B}^{\mathrm{T}}\boldsymbol{\sigma}\,\mathrm{d}V = \int_{\mathcal{B}} \boldsymbol{N}^{\mathrm{T}}\boldsymbol{b}\,\mathrm{d}V + \int_{\partial\mathcal{B}} \boldsymbol{N}^{\mathrm{T}}\boldsymbol{t}\,\mathrm{d}S \tag{21}$$

$$\int_{\mathcal{B}} (\boldsymbol{h}\boldsymbol{h}^{\mathrm{T}} + c\boldsymbol{g}\boldsymbol{g}^{\mathrm{T}})\boldsymbol{e}\,\mathrm{d}V = \int_{\mathcal{B}} \boldsymbol{h}\tilde{\varepsilon}\,\mathrm{d}V \tag{22}$$

The BVP is linearized, hence at nodal points the increments of the primary fields from instant t to instant $t+\Delta t$ are decomposed in such a way:

$$\boldsymbol{a}^{t+\Delta t} = \boldsymbol{a}^t + \Delta\boldsymbol{a} \quad \text{and} \quad \boldsymbol{e}^{t+\Delta t} = \boldsymbol{e}^t + \Delta\boldsymbol{e} \tag{23}$$

Analogically, at integration points we introduce the decomposition of $\boldsymbol{\varepsilon}$, $\boldsymbol{\sigma}$ and $\tilde{\varepsilon}$. The equilibrium equations then become:

$$\begin{aligned}&\int_{\mathcal{B}} \boldsymbol{B}^{\mathrm{T}}(\boldsymbol{\sigma}^t + \Delta\boldsymbol{\sigma})\mathrm{d}V = \\ &= \int_{\mathcal{B}} \boldsymbol{N}^{\mathrm{T}}\boldsymbol{b}^{t+\Delta t}\mathrm{d}V + \int_{\partial\mathcal{B}} \boldsymbol{N}^{\mathrm{T}}\boldsymbol{t}^{t+\Delta t}\,\mathrm{d}S\end{aligned} \tag{24}$$

and the averaging equation has the form:

$$\begin{aligned}&\int_{\mathcal{B}} (\boldsymbol{h}\boldsymbol{h}^{\mathrm{T}} + c\boldsymbol{g}\boldsymbol{g}^{\mathrm{T}})(\boldsymbol{e}^t + \Delta\boldsymbol{e})\mathrm{d}V = \\ &= \int_{\mathcal{B}} \boldsymbol{h}(\tilde{\varepsilon}^t + \Delta\tilde{\varepsilon})\mathrm{d}V\end{aligned} \tag{25}$$

The incremental constitutive relation is derived starting from Equation (7):

$$\begin{aligned}&\Delta\boldsymbol{\sigma} = \boldsymbol{E}^t_{\mathrm{KG}}\boldsymbol{B}\Delta\boldsymbol{a} - \\ &-\left[\mathcal{G}^t_{\mathrm{K}} K\boldsymbol{\Pi}\boldsymbol{\Pi}^{\mathrm{T}} + 2\mathcal{G}^t_{\mathrm{G}} G\boldsymbol{Q}\right]\boldsymbol{\varepsilon}^t\boldsymbol{h}^{\mathrm{T}}\Delta\boldsymbol{e}\end{aligned} \tag{26}$$

where the damage increments have been calculated as:

$$\Delta\omega_{\mathrm{K}} = \mathcal{G}^t_{\mathrm{K}}\boldsymbol{h}^{\mathrm{T}}\Delta\boldsymbol{e} \tag{27}$$

$$\Delta\omega_{\mathrm{G}} = \mathcal{G}^t_{\mathrm{G}}\boldsymbol{h}^{\mathrm{T}}\Delta\boldsymbol{e} \tag{28}$$

and the derivatives are determined at instant t.We can rewrite Equation (24) in a matrix form:

$$\boldsymbol{K}^{\mathrm{KG}}_{aa}\Delta\boldsymbol{a} + \boldsymbol{K}^{\mathrm{KG}}_{ae}\Delta\boldsymbol{e} = \boldsymbol{f}^{t+\Delta t}_{\mathrm{ext}} - \boldsymbol{f}^t_{\mathrm{int}} \tag{29}$$

where:

$$\boldsymbol{K}^{\mathrm{KG}}_{aa} = \int_{\mathcal{B}} \boldsymbol{B}^{\mathrm{T}}\boldsymbol{E}^t_{\mathrm{KG}}\boldsymbol{B}\mathrm{d}V \tag{30}$$

$$\begin{aligned}&\boldsymbol{K}^{\mathrm{KG}}_{ae} = -\int_{\mathcal{B}} \boldsymbol{B}^{\mathrm{T}}[\mathcal{G}^t_{\mathrm{K}} K\boldsymbol{\Pi}\boldsymbol{\Pi}^{\mathrm{T}} + \\ &+ 2\mathcal{G}^t_{\mathrm{G}} G\boldsymbol{Q}]\boldsymbol{\varepsilon}^t\boldsymbol{h}^{\mathrm{T}}\mathrm{d}V\end{aligned} \tag{31}$$

$$\boldsymbol{f}^{t+\Delta t}_{\mathrm{ext}} = \int_{\mathcal{B}} \boldsymbol{N}^{\mathrm{T}}\boldsymbol{b}^{t+\Delta t}\mathrm{d}V + \int_{\partial\mathcal{B}} \boldsymbol{N}^{\mathrm{T}}\boldsymbol{t}^{t+\Delta t}\,\mathrm{d}S \tag{32}$$

$$\boldsymbol{f}^t_{\mathrm{int}} = \int_{\mathcal{B}} \boldsymbol{B}^{\mathrm{T}}\boldsymbol{\sigma}^t\mathrm{d}V \tag{33}$$

In Equation (25) the increment of equivalent strain measure $\Delta\tilde{\varepsilon}$ is computed from the interpolated displacement increment $\Delta\boldsymbol{a}$:

$$\Delta\tilde{\varepsilon} = \left[\frac{\mathrm{d}\tilde{\varepsilon}}{\mathrm{d}\boldsymbol{\varepsilon}}\right]^t \Delta\boldsymbol{\varepsilon} = \left[\boldsymbol{s}^{\mathrm{T}}\right]^t \boldsymbol{B}\Delta\boldsymbol{a} \tag{34}$$

and Equation (25) can be formulated as follows:

$$\boldsymbol{K}_{ea}\Delta\boldsymbol{a} + \boldsymbol{K}_{ee}\Delta\boldsymbol{e} = \boldsymbol{f}^t_{\varepsilon} - \boldsymbol{f}^t_e \tag{35}$$

The matrices and vectors in Equation (35) are similar to the scalar damage formulation, cf. (Peerlings *et al.* 1996):

$$\boldsymbol{K}_{ea} = -\int_{\mathcal{B}} \boldsymbol{h}\left[\boldsymbol{s}^{\mathrm{T}}\right]^t \boldsymbol{B}\mathrm{d}V \tag{36}$$

$$\boldsymbol{K}_{ee} = \int_{\mathcal{B}} (\boldsymbol{h}\boldsymbol{h}^{\mathrm{T}} + c\boldsymbol{g}\boldsymbol{g}^{\mathrm{T}})\mathrm{d}V \tag{37}$$

$$\boldsymbol{f}^t_{\varepsilon} = \int_{\mathcal{B}} \boldsymbol{h}\tilde{\varepsilon}^t\mathrm{d}V \tag{38}$$

$$\boldsymbol{f}^t_e = \boldsymbol{K}_{ee}\boldsymbol{e}^t \tag{39}$$

Eventually, the following system of equations is used:

$$\begin{bmatrix}\boldsymbol{K}^{\mathrm{KG}}_{aa} & \boldsymbol{K}^{\mathrm{KG}}_{ae} \\ \boldsymbol{K}_{ea} & \boldsymbol{K}_{ee}\end{bmatrix}\begin{bmatrix}\Delta\boldsymbol{a} \\ \Delta\boldsymbol{e}\end{bmatrix} = \begin{bmatrix}\boldsymbol{f}^{t+\Delta t}_{\mathrm{ext}} - \boldsymbol{f}^t_{\mathrm{int}} \\ \boldsymbol{f}^t_{\varepsilon} - \boldsymbol{f}^t_e\end{bmatrix} \tag{40}$$

4. ONE-ELEMENT BENCHMARKS

Firstly two benchmarks with one finite element (FE) are computed. These simple tests permit one to observe the behaviour of the isotropic damage at the point level. Better understanding of this model is essential to produce more advanced analyses.

4.1. Tension in one direction

One three-dimensional finite element (FE) with eight nodes is subjected to static tension in one direction. The data for elasticity are as follows: Young's modulus E = 20 000 MPa, Poisson's ratio ν = 0.20.

The normalized elastic energy release rate (Ju 1989) is employed in computations as the loading function, however the Mazars definition (Mazars 1984) and the modified von Mises definition (de Vree *et al.* 1995) for this kind of tension test are all equivalent, i.e. $\kappa^{\mathrm{d}} = \varepsilon_{11}$.We emphasize that damage threshold κ_o = 0.0001 influences one independent history parameter κ^{d}.

The simple modification of scalar theory gives a possibility to adopt of two different damage growth functions, separately for the degradation of bulk modulus K and shear modulus G. All calculated cases are juxtaposed in Table 1.

There are presented symbols used to distinguish a given case and corresponding damage growth data. During the damage evolution ω can grow in different ways. Linear softening law (Peerlings *et al.* 1996):

$$\omega(\kappa^{\mathrm{d}}) = \frac{\kappa_u}{\kappa^{\mathrm{d}}} \frac{\kappa^{\mathrm{d}} - \kappa_o}{\kappa_u - \kappa_o} \tag{41}$$

is introduced in this example in order to illustrate the properties of the isotropic damage model. In the damage evolution firstly κ^{d} exceeds threshold κ_o and next tends to ultimate value κ_u which corresponds to total damage. Here equal or different ultimate values κ_u are assumed for the volumetric and deviatoric degradation. Hence index i = K,G permits one to distinguish the analyzed processes. The cases with identical data for both damage growth functions can be treated as reference (standard scalar damage).

Table 1

Tension in one direction – computed cases

Linear softening		
Symbol of case	Ultimate value of history parameter	
	Volumetric	Deviatoric
lin	$\kappa_u^{\mathrm{K}} = 0.002$	$\kappa_u^{\mathrm{G}} = 0.002$
lin,K	$\kappa_u^{\mathrm{K}} = 0.003$	$\kappa_u^{\mathrm{G}} = 0.002$
lin,G	$\kappa_u^{\mathrm{K}} = 0.002$	$\kappa_u^{\mathrm{G}} = 0.003$
lin,K&G	$\kappa_u^{\mathrm{K}} = 0.003$	$\kappa_u^{\mathrm{G}} = 0.003$
Exponential softening		
Symbol of case	Ductility parameter	
	Volumetric	Deviatoric
exp	$\eta_{\mathrm{K}} = 1000$	$\eta_{\mathrm{K}} = 1000$
exp, K	$\eta_{\mathrm{K}} = 750$	$\eta_{\mathrm{K}} = 1000$
exp, G	$\eta_{\mathrm{K}} = 1000$	$\eta_{\mathrm{K}} = 750$
exp, K&G	$\eta_{\mathrm{K}} = 750$	$\eta_{\mathrm{K}} = 750$

Exponential softening law (Mazars and Pijaudier-Cabot 1989, Peerlings *et al.* 1998):

$$\omega(\kappa^{\mathrm{d}}) = 1 - \frac{\kappa_o}{\kappa^{\mathrm{d}}} \left(1 - \alpha + \alpha e^{-\eta(\kappa^{\mathrm{d}} - \kappa_o)} \right) \tag{42}$$

is also analyzed because this function is adopted in further computations. Here the parameters η and α are responsible for the rate of softening and residual stress which in one dimension tends to $(1-\alpha)E\kappa_o$. In this analysis ductility parameter η is varied. The damage evolution is governed by dominating volumetric or distortion failure. The same numerical stability parameter $\alpha = 0.98$ is assigned. It is also possible to adopt two different damage laws during the failure process, cf. (Wosatko 2008).

Diagrams of strain ε_{11} versus ω_{K} and ω_{G} in the final phase of damage are shown in Figure 1 for chosen cases. They can help one to understand how different damage growth functions influence the results. The non-monotonic function $\omega(\varepsilon_{11})$ in Figure 1(b) results from snapback behaviour which is seen in Figure 2.

In Figure 2 the cases with linear softening are presented. As expected, after the peak, diagrams for *lin,K* and *lin,G* start to decline between diagrams for *lin* and *lin,K&G*. However, the nonlinear character of softening is surprising for the linear damage growth defined for cases *lin,K* and *lin,G*. Moreover, in case *lin,G*, where the deviatoric part has larger κ_u^{G}, arclength control must be used because of the snapback effect. Therefore, it is enough to change the ultimate value κ_u for given volumetric or deviatoric part in order to obtain a nonlinear descend of the stress-strain diagram.

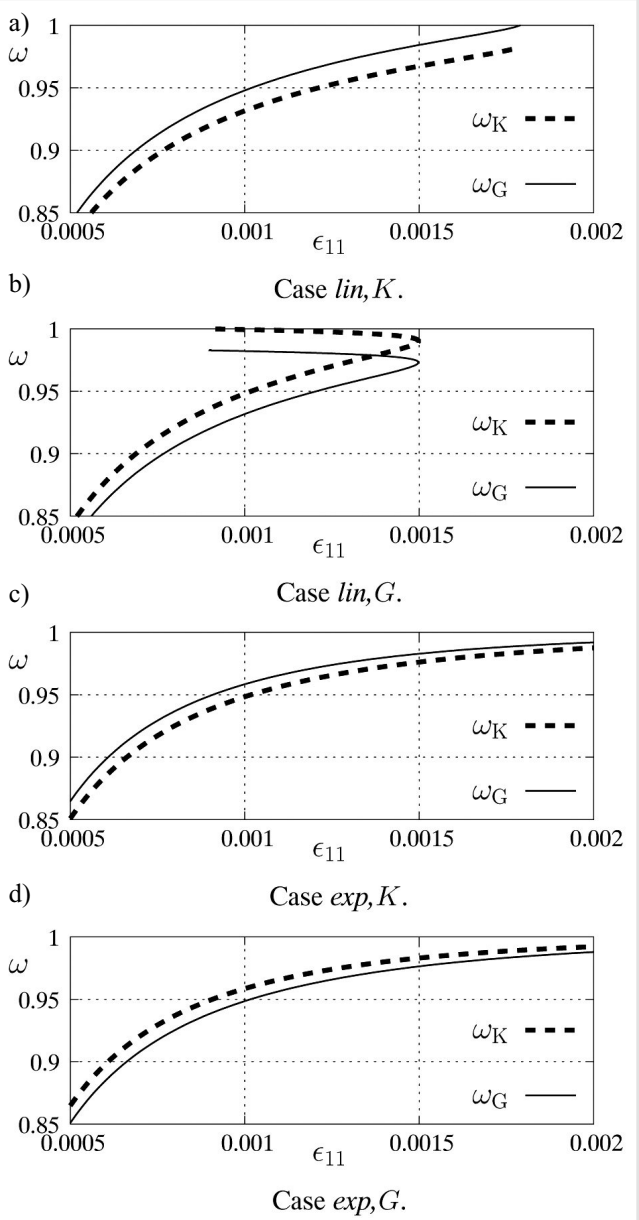

Fig. 1. Development of damage parameters in damage-strain diagrams

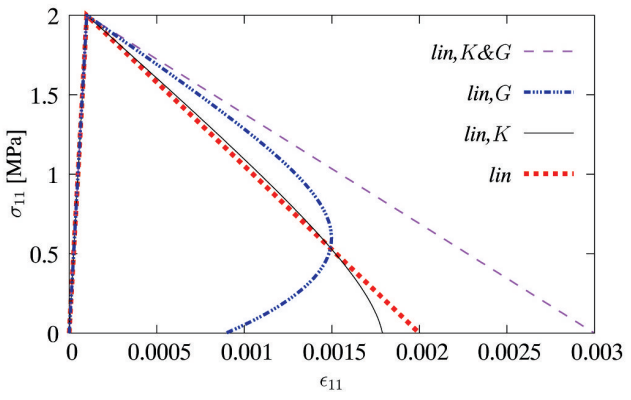

Fig. 2. Influence of ultimate κ_u^i (i = K, G) in linear softening

Figure 3 depicts the diagrams for damage growth functions related to exponential softening. The interpretation is easy since each softening branch has an exponential character. For cases *exp,K* and *exp,G* with different ductility parameters the diagrams run between the extreme cases *exp* and *exp,K&G*. Analogically to the cases with linear functions a certain regularity can be noted. If the fracture energy for the deviatoric part is increased (compare cases *exp* and *exp,G*), it gives a larger difference in response than for larger fracture energy adopted for the volumetric part. It is doubtful to consider the concept of fracture energy only for a chosen part of the stiffness, however in order to simplify the explanations this concept is used here.

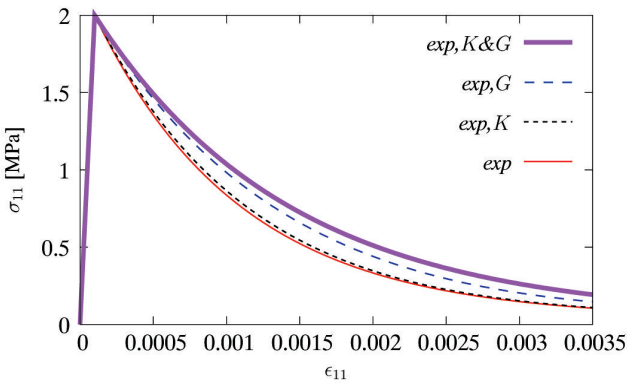

Fig. 3. Influence of ductility parameter η_i (i = K, G) in exponential softening

If $\omega_K \neq \omega_G$ the Poisson's ratio is not constant. It can be computed as (Wosatko 2008):

$$\nu_\omega = \frac{3(1-\omega_K)K - 2(1-\omega_G)G}{2\left[3(1-\omega_K)K + (1-\omega_G)G\right]} \tag{43}$$

so that Poisson's ratio depending on the stiffness degradation is introduced. To distinguish the Poisson's ratio which is given as an elastic material parameter from the one defined in Equation (43) the subscript ω is used. Hence, this new parameter ν_ω is computed during the damage process.

It is shown in Figure 4 how this parameter changes. In the case of linear softening the value of ν_ω drastically tends to a lower or upper limit. These limits can be perceived as controversial results. Such extreme behaviour in simulation and as a consequence nonlinear relation between ε_{11} and σ_{11} seems to be undesirable. A complete degradation for the volumetric part in case *lin,G* gives finally ν_ω equal to –1. On the other hand the zero shear stiffness in case *lin,K* leads to $\nu_\omega = 0.5$ like for incompressible materials, cf. (Carol *et al.* 2002). If exponential softening is used (see Figure 4, case *exp,G*) a smooth drop to zero is observed, but this is not always so. The starting value of ν_ω and also the configuration of the considered test decide on whether ν_ω becomes negative. For quasibrittle materials like concrete generally it is expected that Poisson's ratio tends to 0 during the damage evolution (Carol *et al.* 2002).

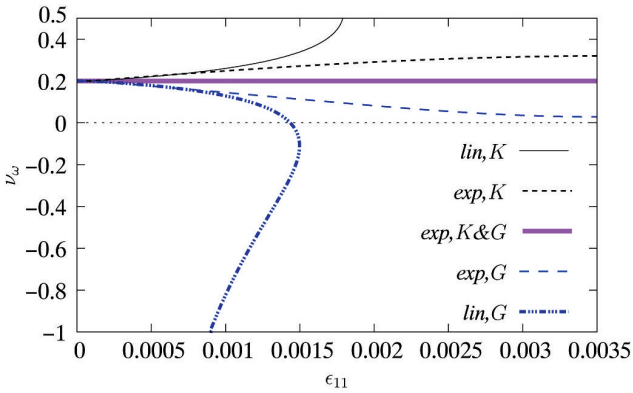

Fig. 4. Sensitivity of Poisson's ratio ν_ω

4.2. Willam's test

The tension-shear test called also Willam's test was computed the first time in (Willam *et al.* 1987). It serves the purpose of verification of inelastic material models at the point level. The results of particular models can be different even if these models in uniaxial tension exhibit a quite similar behaviour, as it was noticed in (Winnicki and Cichoń 1996), so the simulation of tension-shear loading process at the point level completes the numerical analysis of a given model.

One finite element with four nodes in plane stress is subjected to loading in two phases:

I. Uniaxial horizontal tension with vertical contraction due to the Poisson's effect, according to the relation between the strain increments:
$\Delta\varepsilon_{11} : \Delta\varepsilon_{22} : \Delta\gamma_{12} = 1 : -\nu : 0$.
These conditions are obeyed until the tensile strength is attained.

II. Immediately after the tensile strength is reached the change of configuration is enforced. The proportions for the strain increments are arranged as follows:
$\Delta\varepsilon_{11} : \Delta\varepsilon_{22} : \Delta\gamma_{12} = 0.5 : 0.75 : 1$.
This relation induces tension in two directions and additionally a shear strain. As a consequence a rotation of principal strain axes occurs, but the tension regime is preserved.

The test is passed if the maximum principal stress is lower than or at most equal to the given uniaxial tensile strength, cf. (Pivonka *et al.* 2004). The second condition is that finally all stress components should converge to zero.

The set of data is based on Pivonka *et al.* (2004), namely Young's modulus E = 32 000 MPa, Poisson's ratio ν = 0.20, and the remaining parameters are tuned to uniaxial tensile strength f_t = 3 MPa, uniaxial compressive strength f_c = 38.3 MPa and tensile fracture energy G_f = 0.11 N/mm. Modified von Mises definition (de Vree *et al.* 1995) is used, so the ratio between compressive and tensile strength is equal to $k = f_c/f_t \approx 12.77$. The threshold is calculated as the quotient of the tensile strength and Young's modulus $\kappa_o = f_t/E$ = 0.00009375. In this test exponential softening is considered. The first parameter α is equal to 1.0, which means that a complete loss of stiffness is admitted. As previously four cases with different prescribed ductility parameters are considered. The basic case *exp* is for pure scalar damage with $\eta_K = \eta_G$ = 4000. Such a value seems to be unrealistically huge, but results in a fast material failure. Next two cases with different ductilities for the volumetric and deviatoric damage are calculated. The case with more ductile exponential softening for the deviatoric part with parameters η_K = 4000 and η_G = 2000 and as an effect larger volumetric damage ω_K is called *exp,G*. The opposite data η_K = 2000 and η_G = 4000 are used for the case called *exp,K*, where damage for the deviatoric part governs the solution. To complete the results of Willam's test the case *exp,K&G* with both smaller parameters $\eta_K = \eta_G$ = 2000 is also analyzed.

In Figure 5 diagrams for cases *exp* and *exp,K&G* determine bounds for cases with different ductility parameters. The stress-strain diagrams for *exp,K* and *exp,G* are found in exchanged positions comparing with the example of uniaxial tension. It seems surprising, but the Willam test deals with a different loading history. In Figure 5(b) shear relation $\gamma_{12} - \sigma_{12}$ is depicted. A full agreement between diagrams for *exp* and *exp,K*, and also between diagrams for *exp,K&G* and *exp,G* is characteristic for this test. It is connected with the fact that these respective cases have the same parameter G for the deviatoric part.

In Figure 6 the components of stress tensor together with principal stresses are depicted versus strain ε_{11}. The figure shows the results only for the isotropic model taking into account options with different ductility parameters. It is noticed that for case *exp,G* the second principal stress has negative values for large ε_{11}. The final tendency is that all components converge to zero. Figure 7 is plotted for all considered cases. As it is depicted in enlarged sector the zero value is finally reached. If the parameter α is less than 1.0, the residual values remain, see (Wosatko 2008).

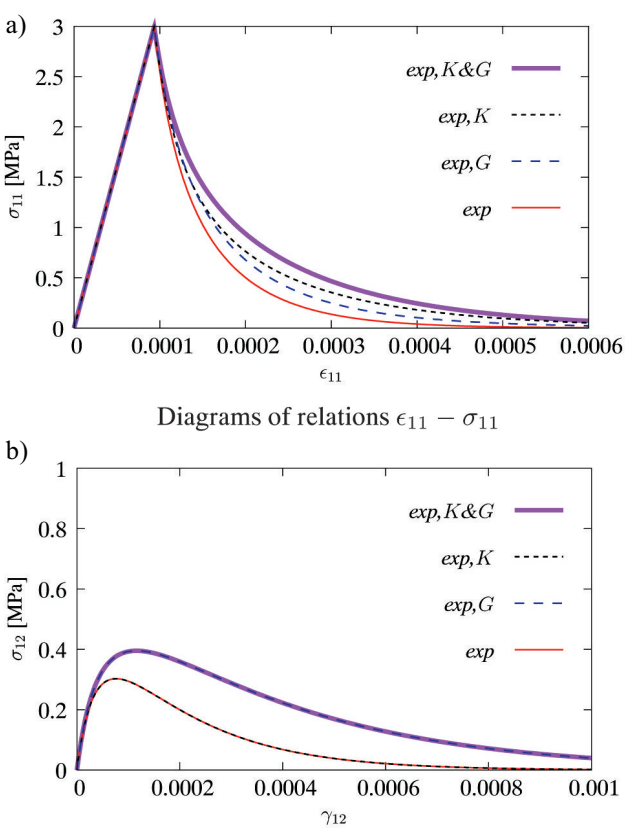

Fig. 5. Willam's test – influence of ductility parameter η_i (i = K, G)

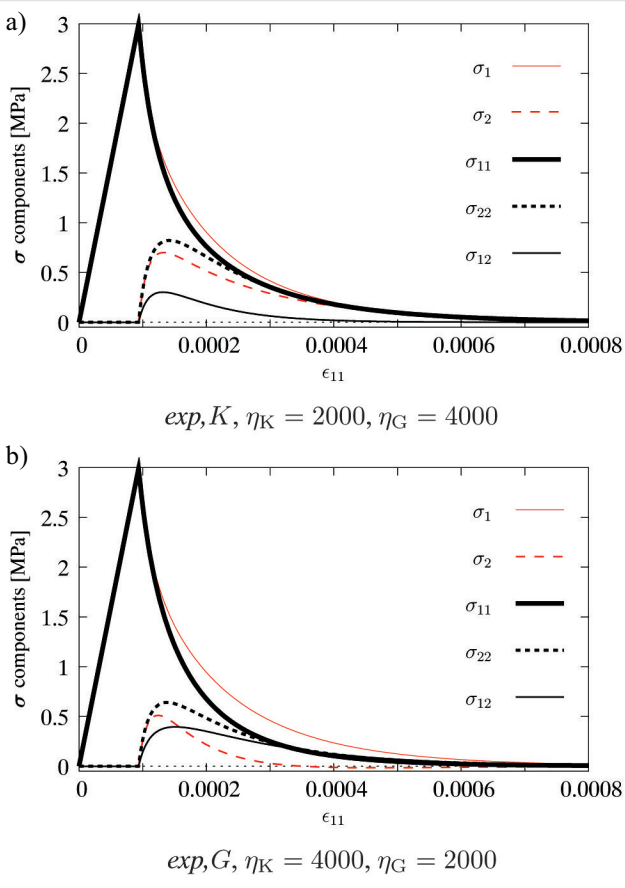

Fig. 6. Willam's test – comparison of stress components

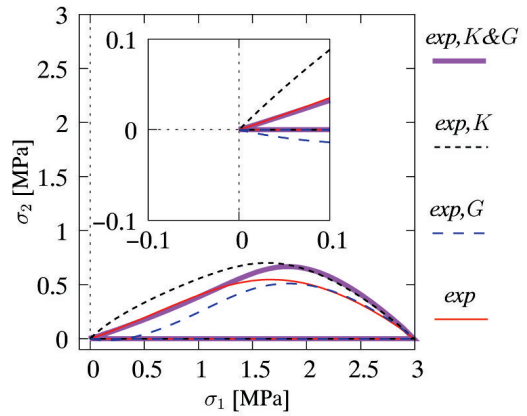

Fig. 7. Willam's test – evolution of principal stresses for isotropic model

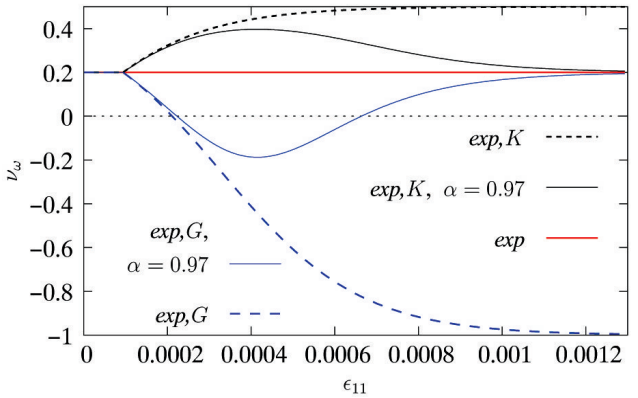

Fig. 8. Willam's test – sensitivity of Poisson's ratio ν_ω. Different relations between parameters α and η_i (i = K, G)

If α is equal to 1 the lower or upper limit of ν_ω is reached, cf. Figure 8. The value of ν_ω can return to the initial one, but for α smaller than 1.0. For quasi-brittle materials a decreasing of Poisson's ratio is expected (see also Carol *et al.* 2002), but negative values are rather non-physical and undesirable. Attention is focused on case *exp,G* where the values of ν_ω are less or at most equal to given in data. It is possible to setup both parameters α and η separately for volumetric and deviatoric part in such way that negative Poisson's ratio is prevented, see (Wosatko 2008).

5. BRAZILIAN TEST

The splitting effect is used to establish the tensile strength in quasi-brittle materials, because the compression between the loading platens induces the perpendicular tensile force action in the middle. This phenomenon and the snapback response in the Brazilian test is not easy to reproduce in numerical computations, because under the platen a plastic zone of slip can appear or damage can localize in a small region. In fact, different mechanical models have been verified numerically using this test, for example in (Chen and Chang 1978) plasticity theories are analyzed, in (Feenstra 1993) rotating crack and plasticity models are confronted, in (Meschke *et al.* 1998) multidirectional kinematic softening damage-plasticity and fixed crack models are tested.

Due to a double symmetry only a quarter of the domain (with radius equal to 40 mm) is considered. The general geometry data are based on (Winnicki *et al.* 2001), but plane strain conditions are assumed. The load is applied to the specimen indirectly via a stiff platen (width – 5 mm, height – 2.5 mm). The platen is perfectly connected with the specimen. In these computations only one mesh shown in Figure 9 is employed, in order to focus on the response of isotropic version of gradient damage. However, mesh insensitivity for scalar gradient damage is widely discussed in (Wosatko 2008). The load acts downwards at the top of the platen. The material data are juxtaposed in Tables 2 and 3. It is shown here that not only the internal length parameter in the gradient model decides about the results of the test, but also other parameters, for instance the choice of the damage growth function, in particular for the volumetric or deviatoric part of damage. Four options of exponential softening are analyzed, where different combinations of values of ductility parameter η decide whether the damage process is more or less brittle. The parameter α equals 0.99 for each case. A snapback response is possible so the test is computed applying the arc length method.

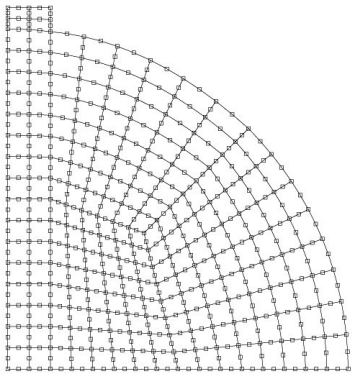

Fig. 9. Mesh for Brazilian test

Table 2

Brazilian test – material model data

Specimen:	damaging
Young's modulus: Poisson's ratio: Equivalent strain measure: Fracture energy: Internal length scale: Threshold:	E_c = 37700 MPa ν = 0.15 modified von Mises, k = 10 G_f = 0.075 N/mm l = 6 mm, i.e. c = 18.0 $\kappa_o = 7.9576 \times 10^{?5}$
Platen:	elastic
Young's modulus: Poisson's ratio:	$E_s = 10 \cdot E_c$ ν = 0.15

Table 3

Brazilian test – computed cases

Symbol of case	η_K	η_G	Damage growth
exp	1200	1200	more intensive
exp,K	600	1200	$\omega_K < \omega_G$
exp,G	1200	600	$\omega_K > \omega_G$
exp,K&G	600	600	less intensive

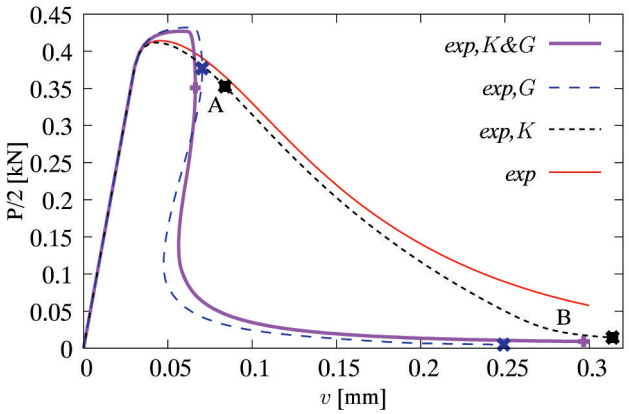

Fig. 10. Brazilian test – influence of ductility parameter ηi (i = K, G), load-displacement diagrams

The load-displacement diagrams in Figure 10 are traced for the four considered cases. It is noticed that for cases *exp,*K and *exp* the softening paths are monotonic and without any snapback. The same value of parameter $\eta_G = 1200$ leads to similar solutions. On the other hand, for cases *exp,*G and *exp,*K&G the snapback response is simulated.

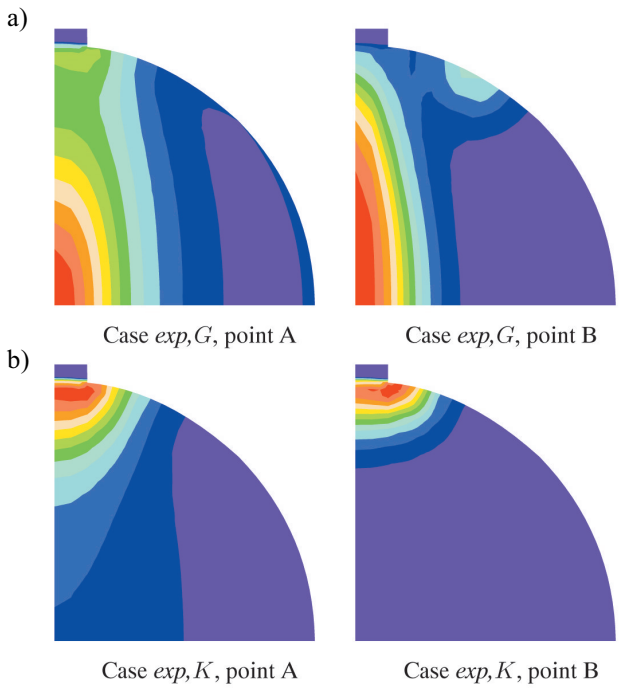

Fig. 11. Brazilian test – averaged strain $\bar{\varepsilon}$

This means that the deviatoric damage is more important in the stiffness degradation and decides about the proper behaviour in the Brazilian test. Contour plots in Figures 11–12 are depicted for the peak and the final state, the respective points A and B are marked in Figure 10.

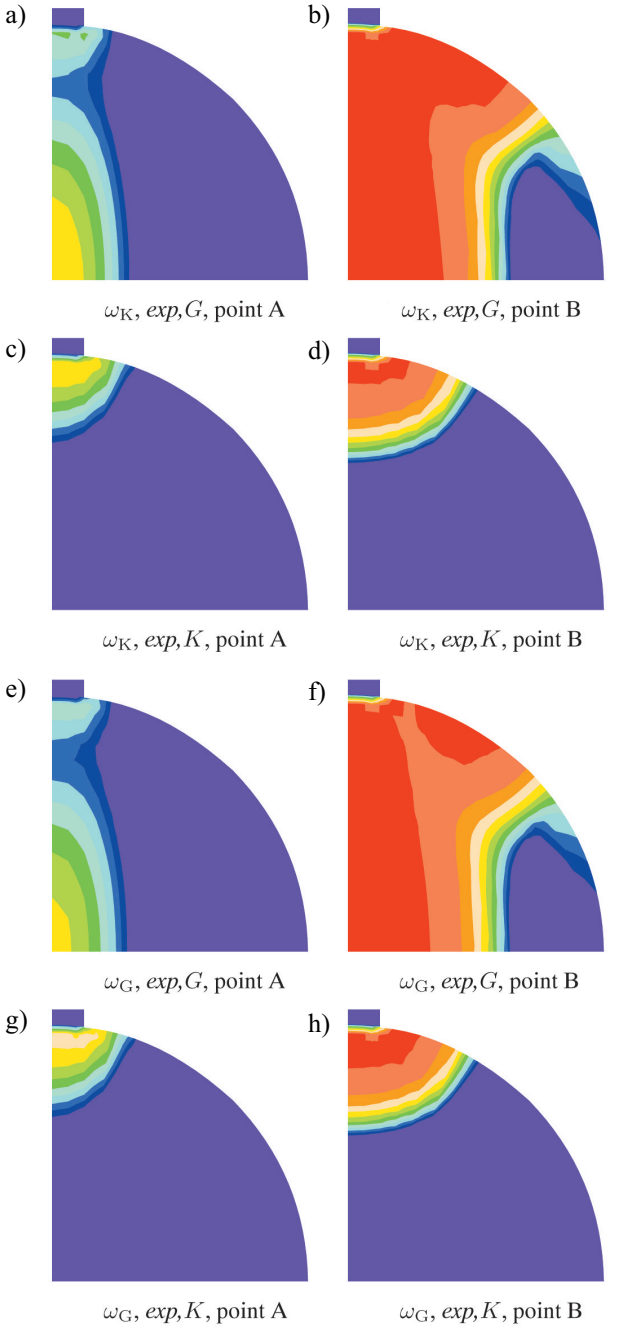

Fig. 12. Damage patterns in Brazilian test

The splitting is obtained only for the cases which correspond to the larger value of fracture energy G_f for the deviatoric part, i.e. the ductility $\eta_G = 600$. It is confirmed by means of Figure 11, where the distributions of averaged strain are plotted for the two stages – points A and B. Therefore the interaction between the compressive loading and the tensile response seems to be transferred via the deviatoric characteristics in the model. Figure 12 shows the

damage patterns for cases *exp,G* and *exp,K*. According to the assumptions included in Table 3, the domination of damage ω_K in case *exp,G* and inversely ω_G in case *exp,K* is noticed. The splitting effect observed for case *exp,G* is expected in the Brazilian test and the coincidence with the decrease of ν_ω during the process is suitable for concrete.

6. FINAL REMARKS

Isotropic damage with the volumetric-deviatoric split is enhanced by averaging equation with second order gradient term. Two different damage growth functions are assumed, however one averaged strain measure is hold. This approach with one strain measure involves one damage loading function. Hence two-field finite element formulation as for the scalar gradient damage is obtained. It is shown even in one FE tension test that one of the features of the isotropic models is that evolving Poisson's ratio is simulated, which is characteristic for degrading quasi-brittle materials. It is however questionable whether its negative values should be admitted in the simulation process. In this model this is not assured, hence only by means of appropriate values for the parameters of the model negative Poisson's ratio can be avoided. However we can overcome this problem, if we apply the model with a restriction similar to proposed in (Ganczarski and Barwacz 2004). The results for all the options of the model satisfy the conditions to pass the Willam test. The case with *exp,G* seems to be the most promising, because for this case the behaviour similar to quasi-brittle materials is obtained.

A total separation of the volumetric and deviatoric parts is possible. In a more general approach two damage loading functions are introduced, two different averaging equations and three-field formulation are derived. A similar approach with total separation of damage parameters is described in (Carol *et al.* 2002), where two damage variables influence two loading functions. Such model is called there bidissipative isotropic model.

Acknowledgments

Valuable discussions with Prof. Jerzy Pamin and Prof. Andrzej Winnicki from Cracow University of Technology are gratefully acknowledged. The computations were performed using the development version of the FEAP program of Prof. R.L. Taylor.

References

Askes H., Pamin J., de Borst R. 2000, *Dispersion analysis and element-free Galerkin solutions of second- and fourth-order gradient-enhanced damage models*. Int. J. Numer. Meth. Engng, 49, pp. 811–832.

Betten J. 1983, *Damage tensors in continuum mechanics*. J. Méc. Théor. Appl., 2(1), pp. 13–32.

Carol I., Rizzi E., Willam K. 2002, *An 'extended' volumetric/deviatoric formulation of anisotropic damage based on a pseudo-log rate*. Eur. J. Mech. A/Solids, 21(5), pp. 747–772.

Chaboche J.-L. 1981, *Continuous damage mechanics: a tool to describe phenomena before crack initiation*. Nuclear Engng. and Design, 64(2), pp. 233–247.

Chen W.F., Chang T.Y.P. 1978, *Plasticity solutions for concrete splitting tests*. ASCE J. Eng. Mech. Div., 104(EM3), pp. 691–704.

Comi C. 2001, *A non-local model with tension and compression damage mechanisms*. Eur. J. Mech. A/Solids, 20(1), pp. 1–22.

Comi C., Perego U. 2001, *Numerical aspects of nonlocal damage analyses*. Revue européenne des éléments finis, 10(2-3-4), pp. 227–242.

de Vree J.H.P., Brekelmans W.A.M., van Gils M.A.J. 1995, *Comparison of nonlocal approaches in continuum damage mechanics*. Comput. & Struct., 55(4), pp. 581–588.

Feenstra P.H. 1993, *Computational aspects of biaxial stress in plain and reinforced concrete*. Ph.D. dissertation, Delft University of Technology, Delft.

Ganczarski A., Barwacz L. 2004, *Notes on damage effect tensors of two-scalar variables*. Int. J. Damage Mechanics, 13, pp. 287–295.

Geers M.G.D. 1997, *Experimental analysis and computational modelling of damage and fracture*. Ph.D. dissertation, Eindhoven University of Technology, Eindhoven.

Ju J.W. 1989, *On energy-based coupled elastoplastic damage theories: constitutive modeling and computational aspects*. Int. J. Solids Struct., 25(7), pp. 803–833.

Ju J.W. 1990, *Isotropic and anisotropic damage variables in continuum damage mechanics*. ASCE J. Eng. Mech., 116(12), pp. 2764–2770.

Kachanov L.M. 1958, *Time of rupture process under creep conditions*. Izd. Akad. Nauk SSSR, Otd. Tekh. Nauk, 8, pp. 26–31 (in Russian).

Krajcinovic D. 1989, *Damage mechnics*. Mechanics of Materials, 8(2–3), pp. 117–197.

Krajcinovic D., Fonseka G.U. 1981, *Continuous damage theory of brittle materials*. ASME J. Appl. Mech., 48(4), pp. 809–824.

Lemaitre J., Chaboche J.-L. 1990, *Mechanics of Solid Materials*. Cambridge University Press, Cambridge.

Litewka A. 1985, *Effective material constants for ortotropically damaged elastic solid*. Arch. Mech., 37(6), pp. 631–642.

Lubliner J., Oliver J., Oller S., Oñate E. 1989, *A plastic-damage model for concrete*. Int. J. Solids Struct., 25(3), pp. 299–326.

Mazars J. 1984, *Application de la mécanique de l'edommagement au comportement non linéaire et à la rupture du béton de structure*. Ph.D. dissertation, Université Paris 6, Paris.

Mazars J., Pijaudier-Cabot G. 1989, *Continuum damage theory – application to concrete*. ASCE J. Eng. Mech., 115, pp. 345–365.

Meschke G., Macht J., Lackner R. 1998, *A damage-plasticity model for concrete accounting for fracture-induced anisotropy*. [in:] de Borst R. *et al.*, editors, Proc. EURO-C 1998 Int. Conf. Computational Modelling of Concrete Structures, vol. 1, pp. 3–12, Rotterdam/ Brookfield. A.A. Balkema.

Murakami S., Ohno N. 1981, *A contiuum theory of creep and creep damage*. [in:] Ponter A.R.S. and Hayhurst D.R., editors, IUTAM Symp., Creep in Structures, pp. 422–444, Berlin, Springer.

Pamin J. 2004, *Gradient-enhanced continuum models: formulation, discretization and applications*. Series Civil Engineering, Monograph 301, Cracow University of Technology, Cracow.

Peerlings R.H.J., de Borst R., Brekelmans W.A.M., de Vree J.H.P. 1996, *Gradient-enhanced damage for quasi-brittle materials*. Int. J. Numer. Meth. Engng, 39, pp. 3391–3403.

Peerlings R.H.J., de Borst R., Brekelmans W.A.M., Geers M.G.D. 1998, *Gradient-enhanced damage modelling of concrete fracture*. Mech. Cohes.-frict. Mater., 3, pp. 323–342.

Pivonka P., Ožbolt J., Lackner R., Mang H.A. 2004, *Comparative studies of 3d-constitutive models for concrete: application to mixed-mode fracture*. Int. J. Numer. Meth. Engng, 60, pp. 549–570.

Skrzypek J., Ganczarski A. 1999, *Modelling of Material Damage and Failure of Structures: Theory and Applications*. Springer, Berlin, New York.

Willam K., Pramono E., Sture S. 1987, *Fundamental issues of smeared crack models*. [in:] Shah S.P. and Swartz S.E. (editors), Proc. SEM-RILEM Int. Conf. on Fracture of Concrete and Rock, pp. 192–207, Bethel, Connecticut. Society of Engineering Mechanics.

Winnicki A., Cichoń Cz. 1996, *Numerical analysis of the plain concrete model prediction for nonproportional loading paths*. [in:] Topping, B.H.V., editor, Advances in Finite Element Technology, pp. 331–339, Edinburgh, Civil-Comp Press.

Winnicki A., Pearce C.J., Bićanić N. 2001, *Viscoplastic Hoffman consistency model for concrete*. Comput. & Struct., 79, pp. 7–19.

Wosatko A. 2008, *Finite-element analysis of cracking in concrete using gradient damage-plasticity*. Ph.D. dissertation, Cracow University of Technology, Cracow.

Wu J.-Y., Li J. 2008, *On the mathematical and thermodynamical descriptions of strain equivalence based anisotropic damage model*. Mechanics of Materials, 40, pp. 377–400.